OXFORD

Cerebral Cortex, 2016; 1–10

doi: 10.1093/cercor/bhw249
Original Article

ORIGINAL ARTICLE

Metabotropic Glutamate Receptor Type 5 (mGluR5) Cortical Abnormalities in Focal Cortical Dysplasia Identified In Vivo With [^{11}C]ABP688 Positron-Emission Tomography (PET) Imaging

Jonathan M. DuBois[1], Olivier G. Rousset[2], Marie-Christine Guiot[1,3], Jeffery A. Hall[1], Andrew J. Reader[4,5], Jean-Paul Soucy[4,6], Pedro Rosa-Neto[1,4,7], and Eliane Kobayashi[1]

[1]Department of Neurology and Neurosurgery, Montreal Neurological Institute, McGill University, 3801 University Street, Montreal, Quebec, Canada H3A 2B4, [2]Division of Nuclear Medicine and Molecular Imaging, Johns Hopkins University, Baltimore, MD 21287, USA, [3]Department of Pathology, McGill University, Montreal, Quebec, Canada H3A 2B4, [4]PET Unit, McConnell Brain Imaging Center, Montreal Neurological Institute, McGill University, Montreal, Quebec, Canada H3A 2B4, [5]Division of Imaging Sciences and Biomedical Engineering, King's College London, St. Thomas' Hospital, London SE1 7EH, UK, [6]Bio-Imaging Group, PERFORM Centre, Concordia University, Montreal, Quebec, Canada H4B 1R6, and [7]Translational Neuroimaging Laboratory, McGill Center for Studies in Aging, Douglas Mental Health University Institute, McGill University, Montreal, Quebec, Canada H4H 1R3

Address correspondence to Eliane Kobayashi. Email: eliane.kobayashi@mcgill.ca

Abstract

Metabotropic glutamate receptor type 5 (mGluR5) abnormalities have been described in tissue resected from epilepsy patients with focal cortical dysplasia (FCD). To determine if these abnormalities could be identified in vivo, we investigated mGluR5 availability in 10 patients with focal epilepsy and an MRI diagnosis of FCD using positron-emission tomography (PET) and the radioligand [^{11}C]ABP688. Partial volume corrected [^{11}C]ABP688 binding potentials (BP_{ND}) were computed using the cerebellum as a reference region. Each patient was compared to homotopic cortical regions in 33 healthy controls using region-of-interest (ROI) and vertex-wise analyses. Reduced [^{11}C]ABP688 BP_{ND} in the FCD was seen in 7/10 patients with combined ROI and vertex-wise analyses. Reduced FCD BP_{ND} was found in 4/5 operated patients (mean follow-up: 63 months; Engel I), of whom surgical specimens revealed FCD type IIb or IIa, with most balloon cells showing negative or weak mGluR5 immunoreactivity as compared to their respective neuropil and normal neurons at the border of resections. [^{11}C]ABP688 PET shows for the first time in vivo evidence of reduced mGluR5 availability in FCD, indicating focal glutamatergic alterations in malformations of cortical development, which cannot be otherwise clearly demonstrated through resected tissue analyses.

Key words: [^{11}C]ABP688, epilepsy, focal cortical dysplasia, metabotropic glutamate receptor type 5, positron-emission tomography

Introduction

Focal cortical dysplasia (FCD), a common cause of drug-resistant epilepsy, is histologically characterized by cortical dyslamination and presence of dysmorphic neurons, including balloon cells (Taylor et al. 1971; Blumcke et al. 2011). Lineage marker protein expression studies in FCD specimens indicate that balloon cells derive from the radial glial progenitor cells in the telencephalic ventricular zone, most carrying a glutamatergic, and therefore excitatory, neurochemical phenotype (Lamparello et al. 2007).

Metabotropic glutamate receptor type 5 (mGluR5) is a post-synaptic G-protein coupled receptor that mediates neuronal excitability (Conn and Pin 1997; Anwyl 1999). mGluR5 plays a key role in cortical development, neurogenesis, cell survival, and regulation of morphogenesis (Catania et al. 2007). In addition, several lines of evidence support a role of mGluR5 in epileptogenesis. mGluR5 downregulation has been described after amygdala kindling and in the pilocarpine mesial temporal lobe epilepsy models (Akbar et al. 1996; Kirschstein et al. 2007). A serial [^{11}C]ABP688 positron-emission tomography (PET) study in pilocarpine-treated rats demonstrated binding changes during the silent period (i.e., epileptogenesis), with pronounced and diffuse reduction of binding following status epilepticus that resolved in all locations except in the hippocampi, as seizures develop in these regions (Choi et al. 2014). The observation of an anticonvulsant effect from mGluR5 antagonism and initiation of persistent epileptiform activity from mGluR5 agonism further indicate an underlying mechanism modulated by this receptor in epileptogenesis, which may contribute to the intrinsic epileptogenicity attributed to malformations of cortical development (Palmini et al. 1995; Chassoux et al. 2000; Merlin 2002; Catania et al. 2007; Bianchi et al. 2009).

Whereas surgical specimens resected from patients with FCD show mGluR5 abnormalities in dysmorphic neurons and balloon cells (Aronica et al. 2003), it remains unclear whether such abnormalities can be identified in vivo. In addition, as with any information obtained exclusively through resected tissue, it is unknown whether mGluR5 abnormalities could be a diffuse cortical characteristic of patients with FCD or limited within the boundaries of the epileptogenic lesion.

Therefore, our primary goal was to investigate in vivo mGluR5 abnormalities in patients with FCD using [^{11}C]ABP688, a PET tracer that binds selectively to the mGluR5 allosteric site allowing whole brain imaging of its availability (Ametamey et al. 2007; Treyer et al. 2007). Demonstrating the possibility to detect mGluR5 abnormalities in vivo could have important clinical implications not only for diagnosis of malformations of cortical development as an underlying cause of seizures (i.e., finding occult or subtle lesions not clearly depicted through anatomical imaging) but also as a biomarker for future pharmacological interventions through identification of populations at higher risk for acquired epilepsies, in whom halting of epileptogenesis and prevention of epilepsy could be attempted.

In order to ensure accurate comparisons between the FCD lesion and healthy cortex, we developed a surface-based analysis with a data-driven partial volume correction method. This method has been instrumental for identifying regional differences related to mGluR5 availability in cortical and subcortical structures (DuBois et al. 2016) and to ensure accurate comparisons across FCD and healthy tissue accounting for location, magnitude, and extent of abnormalities. Furthermore, here we provide information about cortical mGluR5 immunoreactivity for patients who underwent surgical resection and to whom surgical specimens are available for analysis.

Material and Methods

Subjects

We studied 10 patients with focal epilepsy and an MRI diagnosis of FCD investigated at the Montreal Neurological Hospital (Table 1). Five patients underwent surgery and had pathological diagnosis of FCD type IIb or type IIa. Four operated patients are currently seizure-free (Engel I, mean follow-up, 5 years and 9 months, Table 1), while the fifth patient experienced recurrent seizures (Engel II) and relocated medical care 1.5 years ago, at which point follow-up information became unavailable.

Thirty-three healthy subjects (range = 20–77 y/o; males, n = 18, 47.4 ± 17.7 y/o; females, n = 15, 46.2 ± 18.9 y/o) were recruited via university advertisements. Exclusion criteria included: personal or first-degree relative history of axis I psychiatric disorders, chronic use of CNS active medications or illicit drugs, pregnancy/breastfeeding, present or past cigarette usage, history of neurological or medical disorders, and MRI contraindications. The study was approved by the Montreal Neurological Institute Research Ethics Board. All subjects provided written informed consent prior to participation in the study.

PET Acquisition and Reconstruction

[^{11}C]ABP688 was synthetized using the same methodology as in our previous studies (Elmenhorst et al. 2010; DuBois et al. 2016). [^{11}C]ABP688 was administered as a slow bolus injection through an intravenous line at the antecubital region (injected dose/activity = 356.7 ± 25.2 MBq; specific activity = 13.6 ± 6.3 GBq/μmol, unavailable for 10 of the controls). Immediately following injection, a 1-h dynamic emission scan was acquired in 3D list mode.

Six patients and 7 controls were scanned in the Siemens ECAT EXACT HR+ scanner [approximate resolution, 6 mm full width at half maximum (FWHM)]. The remaining subjects (4 patients, 26 controls) were scanned with the Siemens High Resolution Research Tomograph (HRRT, approximate resolution of 3 mm FWHM).

After correction for attenuation, scatter, and decay, data were reconstructed by filtered back-projection. The reconstructed time-series was 128 × 128 × 63 voxels (2.45 mm pixels) for the HR+ and 256 × 256 × 207 voxels (1.21875 mm pixels) for the HRRT.

To combine data from both scanners, the HRRT images were blurred with an anisotropic Gaussian kernel of 5.7 × 5.7 × 6.7 mm FWHM, based on findings from an in-house phantom study (unpublished data). The anisotropic Gaussian

Table 1 Clinical information

Patient	Age	Sex	FCD location	Last sz prior to scan (days)	AEDs	Age at sz onset/duration of epilepsy (years)	Surgery follow-up (years), Engel class	Pathology	PET scanner
1	39	F	L lateral frontal	180	LEV, LMT, CLB, CBZ	3/36	No	N/A	HR+
2	56	M	R mesial parietal/ posterior cingulate	1	CBZ, LEV, CLB	8/48	6 y, Engel I	FCD IIb	HR+
3	25	M	R superior temporal	4	CBZ	8/17	6 y9 m, Engel I	FCD IIb	HRRT
4	20	F	L superior temporal	1	CLB	14/6	No	N/A	HRRT
5	19	F	R parahippocampal	11	VA, LEV, PB	15/4	6 y11 m, Engel II	FCD IIa	HR+
6	31	F	L posterior cingulate/mesial parietal	1	LMT, DPH, CLB	16/15	No	N/A	HR+
7	39	F	L mesial orbitofrontal	30	None (LMT discontinued at admission)	34/5	No	N/A	HR+
8	29	M	R frontal pole	1	VA, OXC, CLB	0.4/29	4 y3 m, Engel I	FCD IIb	HRRT
9	41	F	L posterior fusiform gyrus	6	LMT, PB, CLB	12/29	No	N/A	HR+
10	38	M	R inferior frontal	1	CBZ, CLB	17/21	5 y1 m, Engel I	FCD IIb	HRRT

F, female; M, male; L, left; R, right; sz, seizure; AED, antiepileptic drug; LEV, levetiracetam, LMT, lamotrigine; CBZ, carbamazepine; CLB, clobazam; DPH, diphenylhydantoine; VA, valproic acid; OXC, oxcarbazepine; PB, phenobarbital.

kernel used here was similar to previously published methods using an isotropic Gaussian kernel of 6 mm FWHM (van Velden et al. 2009).

MRI Acquisition and Processing

As described previously in DuBois et al. (2016), a 3D T1-weighted MPRAGE sequence (1 mm^3 voxel size, 256 × 256 × 256 matrix; TE = 2.98; TR = 2300; TI = 900 ms; flip angle = 9) was acquired for each subject using a Siemens Trio 3 T scanner. MRI data were analyzed with FreeSurfer (www.surfer.nmr.mgh.harvard.edu, version 6.0 beta) (Dale et al. 1999; Fischl et al. 1999a, 2002) in order to perform subvoxel reconstruction of the pial surface and gray matter/white matter boundary (i.e., the white matter surface). The initial surface reconstruction was then manually inspected and corrected for errors due to incomplete removal of nonbrain tissue or inadequate intensity normalization. At each vertex on the final white matter surface, cortical thickness was estimated as the closest distance between the white matter surface to the pial surface (Fischl and Dale 2000). The subject surface was registered to symmetric and asymmetric average templates for subsequent analysis and visualization (Fischl et al. 1999b; Greve et al. 2013).

Boundary-based rigid-body registration was utilized to accurately align the MRI and the time-averaged raw PET images by fitting the white matter surface to the maximum of the radioactivity gradient (Greve and Fischl 2009). Each subject's registration was visually inspected and manually adjusted when necessary. Using the cortical thickness information, PET data were then sampled from the middle of the cortex, halfway between the white matter and pial surfaces (Greve et al. 2014; DuBois et al. 2016).

Correction for partial volume error was performed using a data-driven, region-based per-voxel partial volume correction method, as described in DuBois et al. (2016). First, time-averaged raw PET data were sampled to the surface and blurred at 10 mm FWHM (Greve et al. 2014). For each hemisphere, high, low, and mid-range clusters were created by setting thresholds one standard deviation above and below the mean radioactivity. Clusters were defined as a set of continuous vertices within the threshold range and with a surface area greater than 200 mm^2 (DuBois et al. 2016). These cortical regions were then sampled back to the subject's MRI volume space and combined with subcortical gray and white matter segmentations (Desikan et al. 2006). The geometric transfer matrix method was used to obtain the partial volume corrected PET values for each region (Rousset et al. 1998). The resulting values were then used to perform per-voxel correction for the whole brain (Thomas et al. 2011).

Binding Potential Analysis

Following PVC, [^{11}C]ABP688 nondisplaceable binding potentials (BP_{ND}) were estimated using the simplified reference tissue model (with the cerebellar gray matter as reference region) and a basis function implementation of voxel-wise parametric mapping (Lammertsma et al. 1996; Gunn et al. 1997; Innis et al. 2007; Elmenhorst et al. 2010). Despite the presence of mGluR5 in the cerebellar cortex, several lines of evidence indicate that specific [^{11}C]ABP688 binding in the cerebellar cortex is negligible, including in vitro and in vivo imaging of [^{11}C]ABP688 binding in humans and animals (Elmenhorst et al. 2010; Milella et al. 2011), and human postmortem analysis of mGluR5 mRNA (Daggett et al. 1995) and protein expression (Deschwanden et al. 2011).

FCD Manual Labeling Procedure

Three labels were created for each patient to encompass the lesion, as well as the perilesional and contralateral cortex in relation to the lesion (Fig. 1). The "FCD label" was manually traced along the white matter surface representation in volume space using each patient's MRI. Characteristics such as cortical thickness, blurring of the gray/white matter junction, and abnormal gyrification were used to estimate the extent of the lesion. When available, the clinical T2-weighted MRI was also utilized. All tracings were reviewed and corrected, when needed, by an experienced epileptologist. Each labeled voxel was assigned to the nearest white matter surface vertex. An automatic topological closing operation was used to fill any

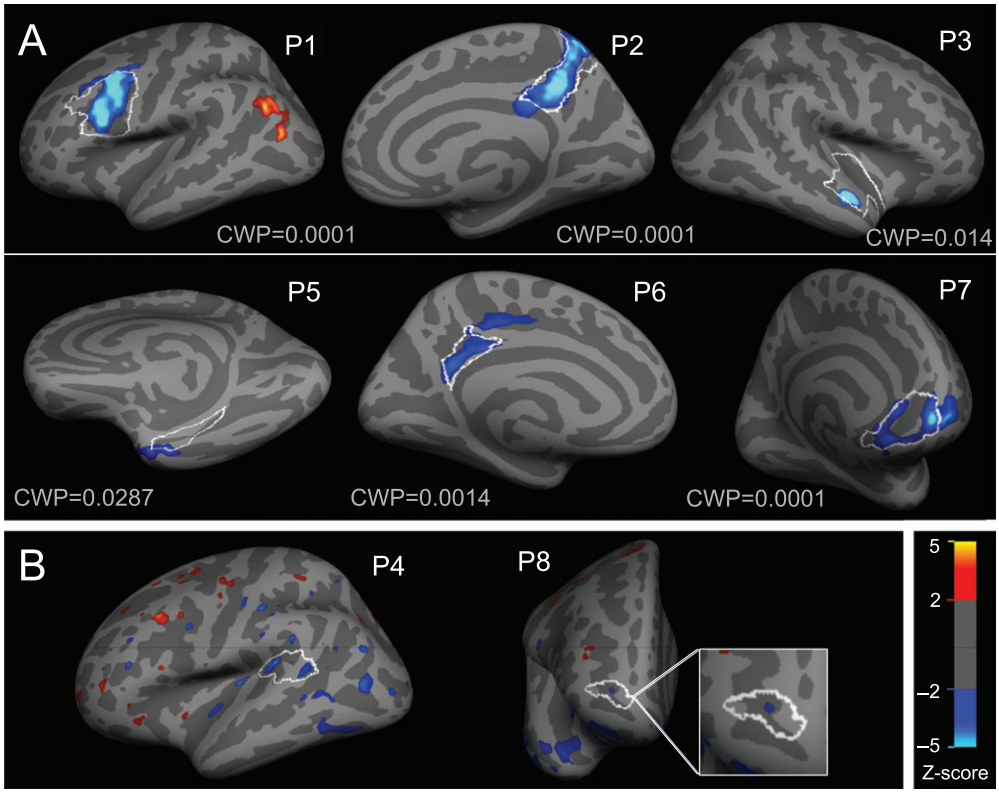

Figure 1. Individual vertex-wise z-score maps showing reduced [^{11}C]ABP688 BP_{ND} in FCD lesions. Results are displayed on each patient's inflated cortical surface, with light gray regions indicating gyri and dark regions indicating sulci. FCD boundaries from manual labeling are displayed as a white outline. Blue-teal colors indicate regions with lower BP_{ND} as compared to controls, whereas red-yellow colors indicate regions with higher BP_{ND} compared to controls. (*A*) Six patients showed clusters of decreased [^{11}C]ABP688 BP_{ND} differences within the lesion boundaries, which remained significant after correction for multiple comparisons (corresponding cluster-wise *P*-value is indicated as CWP). (*B*) Two patients showed small lesional clusters of reduced [^{11}C]ABP688 BP_{ND} that (displayed here at $P < 0.05$), were not significant after correction for multiple comparisons.

holes created by gaps in the volume label or the subvoxel resolution of the surface. The "perilesional label" was created to account for the possibility of lesions extending beyond the MRI-visible abnormalities, by dilating each surface lesion label by approximately 10 mm in all directions followed by subtraction of the FCD label area. The "contralateral lesion label" was created by sampling the surface lesion label to the contralateral surface using average symmetrical atlas. This surface-based approach was used to ensure that the contralateral lesion label was sampled to the appropriate cortical anatomy (Greve et al. 2013).

Statistical Analyses

Vertex-wise group comparisons of BP_{ND} were conducted in the average surface space using the FreeSurfer software package. Once sampled to the surface, BP_{ND} images were blurred at 5 mm FWHM and 2-tailed Z-tests were computed between each patient and the entire control group. Multiple comparisons correction for the number of vertices was carried out with a cluster-based Monte Carlo simulation (cluster-wise $P < 0.05$) (Hagler et al. 2006). In order to assess the distribution of extralesional vertex-wise findings, we calculated the Euclidian distance along the cortical surface originating from the maximum vertex within the extralesional cluster and the nearest edge of the lesion label.

Z-tests were used to determine differences between average BP_{ND} within a given region-of-interest (ROI) for each patient and homotopic areas in the control group. Based on the results of the vertex-wise analysis, Z-scores were converted to one-tailed *P*-values for false discovery rate correction for multiple comparisons (Benjamini et al. 2006). Analyses and figures were generated with the R statistical software package (R Core Team 2013).

Surgical Specimens Analysis

FCD was confirmed based on the presence of cortical dyslamination and dysmorphic neurons with balloon cells (Type IIb) or without balloon cells (Type IIa) (Blumcke et al. 2011) using formalin-fixed paraffin-embedded tissue from surgery (Blumcke et al. 2011). Neuropathology protocol included immunostaining for neuronal nuclear antigen NeuN, MAP2, synaptophysin, glial fibrillary acidic protein GFAP, Nissl (Luxol Fast Blue/Cresyl Violet), and Bielschowsky stainings.

mGluR5 staining (anti-mGLUR5 C-terminus antibody, Millipore Chemicon 06–451, 1:100) was performed in 5 µm slices adjacent to those used for clinical diagnosis. Immunohistochemistry was performed on a Benchmark XT stainer (Ventana Medical System): after deparaffinization, sections were pretreated with cell conditioning 1 buffer, the primary antibody was applied for 32 min and the Ultraview DAB kit was used. Slides were digitalized using an Aperio scan-scope system and image analysis was performed using Spectrum software.

A descriptive qualitative analysis of mGluR5 immunostaining was conducted (Aronica et al. 2003). Cells (balloon cells,

dysmorphic neurons and normal neurons) and neuropil were visually analyzed and rated for the immunoreactivity pattern as negative, mild, moderate, and strong (Aronica et al. 2003).

Results

Vertex-wise Analysis of [^{11}C]ABP688 BP_{ND}

Reduced BP_{ND} was found within the lesion in 8/10 patients, which remained significant in 6 patients after cluster-wise correction for multiple comparisons (see Fig. 1; Supplementary Table 1). No patients showed clusters of increased BP_{ND} within the lesion. Eight out of 10 patients showed a median of 3 extralesional areas of increased or decreased BP_{ND}, which were diffusely scattered throughout the ipsilateral and contralateral cortices (Fig. 2). These extralesional clusters were mainly found in 3 patients, at variable distance from the lesion (Fig. 2). Although the HRRT PET data were blurred to match the HR+ resolution, extralesional BP_{ND} abnormalities were more frequent in patients imaged with the HR+ scanner.

ROI Analysis of [^{11}C]ABP688 BP_{ND}

Confirming vertex-wise analysis, significantly lower lesional BP_{ND}, was found in 6/10 patients as compared to the homotopic cortex in healthy controls (z-scores ranging from −5.58 to −2.32; see Supplementary Table 1; Fig. 3). No differences were found between patients and controls in the perilesional or the contralateral lesion labels. These ROI results differed slightly from the vertex-wise results in that patient #5 (significantly reduced BP_{ND} within a small anterior portion of the lesion—Fig. 1) did not show a significant difference in the ROI analysis, which can be understood by the extensive portion of the lesion extending posteriorly and that does not show any BP_{ND} abnormality. On the other hand, patient #4 showed significantly reduced lesional BP_{ND} in the ROI analysis (Fig. 3), but only small nonsignificant vertex-wise clusters of decreased BP_{ND} in the ipsilateral temporal lobe, including some located within the lesion (Fig. 1).

Epilepsy duration showed no association with mean BP_{ND} in the FCD lesion ($r = 0.17$, $n = 8$, $P = 0.65$). Considering the possible effect of extracellular glutamate levels fluctuations in [^{11}C]ABP688 BP_{ND} (Zimmer et al 2015), we further analyzed whether there was a relationship between the last seizure and the scan date. Likewise, no correlation was found between the number of days since the last seizure and BP_{ND} in the FCD lesion ($r = 0.19$, $n = 8$, $P = 0.60$).

mGluR5 Immunohistochemistry

We found a high degree of intra/intersubject variability in mGluR5 immunoreactivity within the lesions. There was weak to strong neuropil staining; dysmorphic neurons as well as balloon cells, however, most often showed negative or weak immunoreactivity, with isolated and at times rare cells showing moderate or strong immunoreactivity. Intracellular and membrane staining was variable across sections and cells, with one patient showing intranuclear immunoreactivity in isolated dysmorphic and balloon cells (Fig. 4F). Normal neurons from cortical regions at the border of the resections showed normal strong cytoplasmic mGluR5 immunoreactivity (Aronica et al. 2003). Altogether, the resulting cortical pattern was of weak-moderate mGluR5 immunoreactivity derived from neuropil staining (Fig. 4A,C,E,G), with negative-mild intracellular immunoreactivity in portions of the lesion with most severe abnormalities (i.e., with higher concentration of balloon cells, Fig. 4B,H).

Discussion

In this study, we identified for the first time in vivo mGluR5 abnormalities in FCD lesions using [^{11}C]ABP688 PET. Reduced BP_{ND} within the FCD was observed in 70% of patients using a combination of vertex-wise and ROI analyses. While no BP_{ND} differences were found in perilesional or contralateral cortices in ROI analysis compared to homotopic regions in healthy controls (Fig. 3), vertex-wise whole cortex analysis showed mGluR5

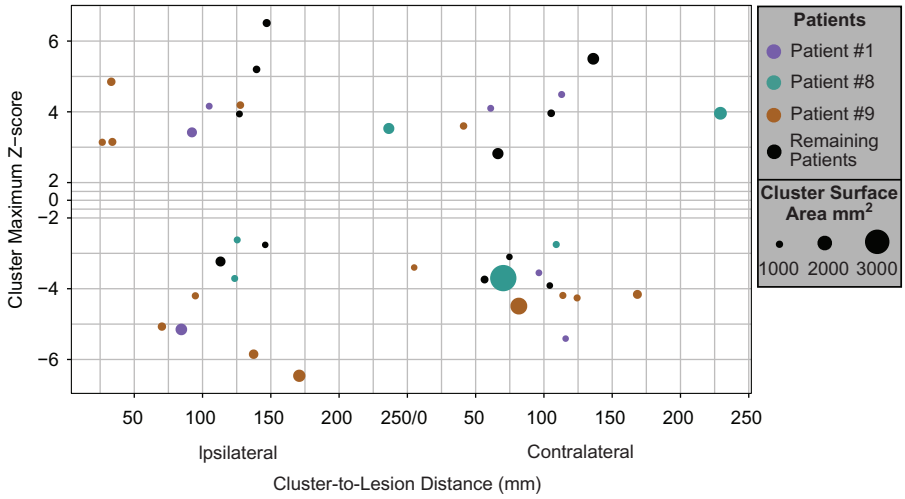

Figure 2. Distribution of significant extralesional clusters of [^{11}C]ABP688 BP_{ND} differences. Scattered clusters of increased and decreased [^{11}C]ABP688 BP_{ND} in the ipsi- and contralateral hemispheres observed in our group of patients can be primarily accounted for by 3 subjects. The x-axis displays the percent of the maximum Euclidian distance along the cortical surface between the vertex of max Z-score value within each significant cluster and the nearest edge of the ipsilateral lesion label. In the contralateral hemisphere, distance is calculated between the vertex of max Z-score value within each significant cluster and the nearest edge of the contralateral lesion label. The y-axis displays the maximum Z-score of each significant extralesional cluster (the portion of the y-axis between 2 and −2 is compressed because there are no significant z-scores within this threshold). The diameter of the circle represents the surface area of each cluster, ranging from 1000–3000 mm^2. Separate colors distinguish the 3 patients with the largest number of extralesional clusters (patient #1—purple, patient #8—green, patient #9—brown), while extralesional clusters in the remaining 5 patients are displayed altogether in black.

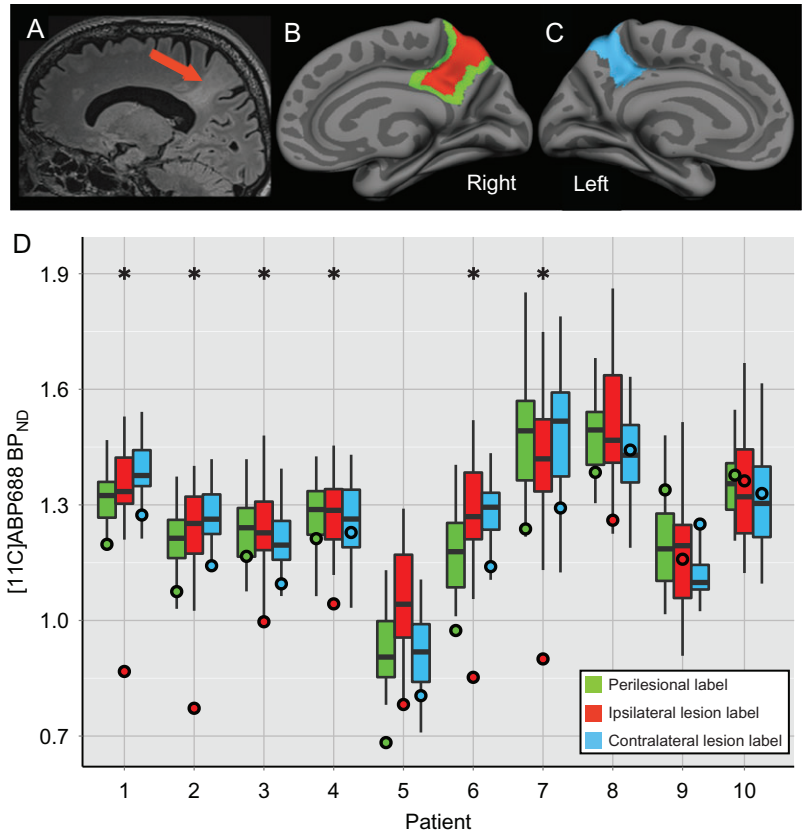

Figure 3. Reduced [^{11}C]ABP688 BP_{ND} in FCD compared to homotopic regions in controls. (A–C) Illustrate the labeling procedure in a patient with a parietal FCD (patient #2): (A) sagittal slice of a T2-FLAIR MRI image showing the lesional cortex (indicated by the red arrow); (B) the ipsilateral right hemisphere of the semi-inflated pial surface with the lesion label shown in red and the perilesional label shown in green, and (C) the contralateral left hemisphere of the semi-inflated pial surface displaying the contralateral lesion label in blue. (D) X-axis indicates the patient number; Y-axis indicates [^{11}C]ABP688 BP_{ND} values. The boxplots display the average [^{11}C]ABP688 BP_{ND} values within homotopic cortical regions of the control group corresponding to the perilesional (green), the ipsilateral lesion (red), and the contralateral lesion (blue) labels for each patient. The boxplot whiskers extend to the highest or lowest data point within 1.5 times the inter-quartile range. Each circle displays the average BP_{ND} for the corresponding patient for the three ROIs. *$P < 0.05$.

abnormalities within the visible lesion sometimes extending to the surrounding cortex (Fig. 1).

Reduced BP_{ND} may indicate reduced mGluR5 tissue concentration or a reduction of [^{11}C]ABP688 affinity to mGluR5 caused by receptor internalization, conformational changes, anomalous receptor isoforms, or excessive concentrations of endogenous ligands. Reduced BP_{ND} observed in our patients can be first explained by mGluR5 interactions with glutamate, found to be at high levels in the extracellular compartment in the epilepsy focus (During and Spencer 1993). While [^{11}C]ABP688 binds selectively to the mGluR5 allosteric site, glutamate binding to its orthosteric site causes a conformational change that makes the transmembrane allosteric site unavailable (Ametamey et al. 2007; Treyer et al. 2007).

Although it is still unclear to what degree mGluR5 availability fluctuates during and after seizures, microdialysis studies have shown that extracellular glutamate concentrations increase prior to and during a seizure (During and Spencer 1993; Meurs et al. 2008). Interestingly, the two patients who showed no [^{11}C]ABP688 BPND differences in the FCD lesion (i.e., patients #9 and #10), experienced frequent seizures prior to [^{11}C]ABP688 PET scanning. We have previously demonstrated, by combined microdialysis and PET, that [^{11}C]ABP688 BPND is influenced by extracellular synaptic concentration of glutamate (Zimmer et al. 2015). Prior evidence further supports that [^{11}C]ABP688 BP_{ND} can be modulated by extracellular glutamate: administration of a sub anesthetic dose of ketamine, known to elicit glutamate release, caused a 20% decrease in BP_{ND} throughout the brain of healthy controls (DeLorenzo et al. 2014).

Since seizures induce dynamic changes in GABA and glutamate (Rowley et al. 1997) as well as glutamate transporter expression (Hubbard et al. 2016), it is plausible to expect that [^{11}C]ABP688 BPND in FCD might incorporate information regarding extracellular concentration of glutamate. As such, these factors should be taken into account to interpret PET mGluR5 imaging in epilepsy due to the high frequency of seizures (including electrographic seizures) among carriers of an FCD lesion. Many patients with FCD have abundant spiking activity, particularly evidenced when these lesions are targeted with intracranial EEG electrodes.

Patient #10 had not only frequent seizures but also abundant interictal epileptiform discharges, with almost continuous spiking activity found in intracranial EEG monitoring prior to surgery. In addition, patients #9 and #10 experienced frequent nocturnal seizures, which may have interrupted their normal sleep pattern. A recent study showed that sleep deprivation was associated with a global increase in [^{11}C]ABP688 binding, maximal in the medial temporal lobe and cingulate cortex, in healthy individuals (Hefti et al. 2013). While further

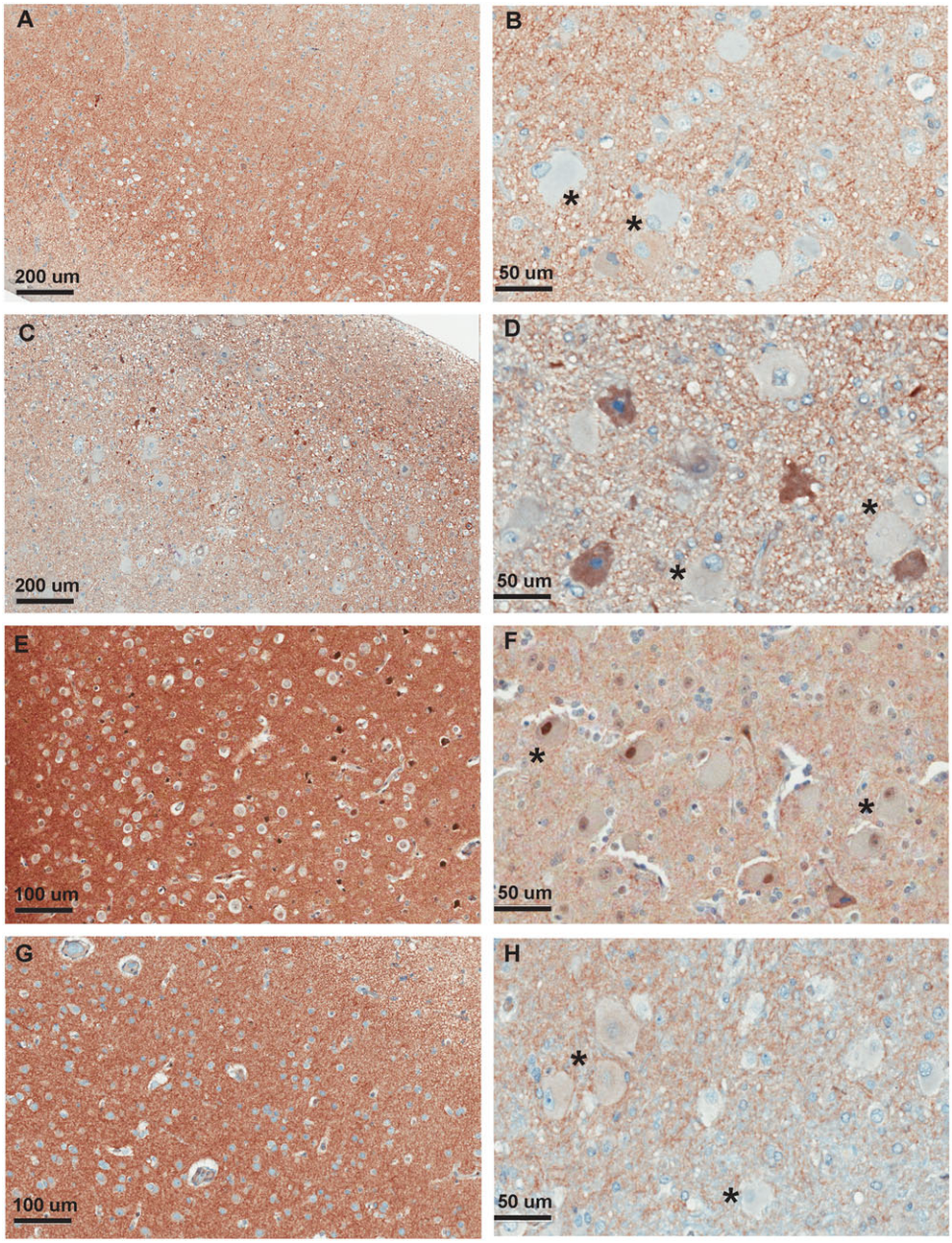

Figure 4. mGluR5 immunohistochemistry in resected FCD IIb tissue. (*A*) Patient #2, objective ×10: Disorganization of the cortex, in which no pyramidal cell layer can be properly identified. There is presence of numerous dysmorphic neurons and balloon cells, with few entrapped neurons strongly stained for mGluR5. (*B*) Patient #2, objective ×40: Detailed view of deeper cortical section in the same slide, with presence of balloon cells (asterix), which are negative for mGluR5, with few entrapped neurons and dysmorphic neurons showing a cytoplasmic pattern of mGluR5 staining. (*C*) Patient #3, objective ×10: Disorganization of the cortex, presence of dysmorphic neurons and rare neurons strongly stained for mGluR5. (*D*) Patient #3, objective ×40: Detailed view of deeper section in the same slide, with presence of mGluR5-negative balloon cells (asterix) and mGluR5-positive neurons. (*E*) Patient #8, objective ×10: Disorganization of the cortex, in which no pyramidal cell layer can be properly identified. Few neurons are strongly stained for mGluR5. (*F*) Patient #8, objective ×40: Detailed view of deeper section of the cortex, with presence of balloon cells (asterix) with either no clear staining or with a strong nuclear mGluR5 staining. (*G*) Patient #10, objective ×10: Disorganization of the cortex, with strong neuropil staining but no mGlur5-positive neurons identified. (*H*) Patient #10, objective ×40: Detailed view of deeper section depicting the transition of cortex/white matter, with presence of balloon cells (asterix) with either absent staining or weak cytoplasmic staining.

investigation is needed to confirm these speculations, it is possible that increased seizure activity alone or combined with sleep deprivation may have obscured localized lesional changes in [^{11}C]ABP688 BPND in these patients.

Furthermore, given its dependency on glutamate concentrations, [^{11}C]ABP688 BP_{ND} might also be related to excitotoxicity. In FCD type IIb, glutamatergic balloon cells with reduced or dysfunctional mGluR5 could potentially result in insufficient postsynaptic modulation of glutamatergic transmission, leading to increased excitotoxicity.

Extralesional areas of increased or decreased BP_{ND} were also observed in some patients, including those who underwent resection of the MRI-visible lesion and who are currently seizure-free. While we cannot fully understand the significance

of these scattered extralesional abnormalities, in this small series of patients it did not seem to implicate in a poor postsurgical prognosis or to highlight additional areas of epileptogenicity.

Our analysis showed that extralesional abnormalities could be found scattered across both hemispheres, but were unevenly represented across subjects (Fig. 2). The patient with the largest number of significant extralesional abnormalities (patient #9) has not been operated. This patient has frequent clusters of seizures and bilateral independent EEG abnormalities, which may suggest cortical abnormalities extending beyond the visible lesion. However, the other two patients who showed a large number of extralesional abnormalities are both seizure-free following resective surgery of the MRI-visible FCD lesion. The reason why patients imaged in the HR+ PET scanner showed a larger number of extralesional abnormalities could be a result of variability in the HR+ scanner, the effect of combining the HR+ and HRRT data sets, or differences inherent to the patients.

Because of its role in cortical development, neurogenesis, cell survival and regulation of morphogenesis, mGluR5 abnormalities in FCD could reflect a developmental feature of the malformed tissue mediated through this receptor that makes these lesions highly epileptogenic, as demonstrated by neurophysiological studies (Palmini et al. 1995; Catania et al. 2007). In a pilocarpine-treated rat model of temporal lobe epilepsy, status epilepticus was associated with a global reduction in [^{11}C]ABP688 BP_{ND} (Choi et al. 2014). Following status, [^{11}C]ABP688 BP_{ND} remained reduced in the hippocampus and amygdala, regions that later developed epileptogenicity and became capable of producing spontaneous seizures in the chronic stage. This suggests a role for mGluR5 in epileptogenesis of previously normal brain regions.

Tissue analysis conducted in a small subsample of our patients who underwent surgical resection of the MRI-visible FCD lesion, showed concordance between mGluR5 immunoreactivity pattern, abnormal histology and [^{11}C]ABP688 PET. mGluR5 immunohistochemistry revealed negative or weak staining of balloon cells and dysmorphic neurons that, despite not being a quantitative measurement of protein levels, suggest that this might be contributory to the in vivo findings with [^{11}C]ABP688. In three operated patients, reduced BP_{ND} within the FCD could be at least partially attributed to the substitution of normal appearing mGluR5-positive neurons by mGluR5-negative or weakly stained abnormal (balloon) cells.

The reason why one operated patient did not show detectable in vivo [^{11}C]ABP688 BP_{ND} abnormalities is unknown since the tissue analysis did not reveal any significant differences compared to other operated patients who had in vivo [^{11}C]ABP688 BP_{ND} abnormalities (Fig. 4*G*,*H*). In vivo binding studies using PET should be carefully interpreted since the binding of the radioligand is influenced by 1) the total amount of protein in the tissue (Morey et al. 2009), 2) the functional state of the receptor (high/low affinity state), and 3) the presence of an endogenous competitor (Chugani et al. 1988; van Wieringen et al. 2013; Zimmer et al. 2015; Vidal et al. 2016).

Furthermore, the quantification or mGluR5 using molecular imaging agents cannot discriminate cellular compartments, but rather provide measures of tissue concentrations (Zimmer et al. 2014). As such, the "normal" [^{11}C]ABP688 binding observed here can be explained by steady-state status of the tissue during the PET scan session (Zimmer et al. 2014). For example, we have previously shown using PET and microdialysis that reduction in tissue glutamate concentrations via activation of glutamate transporter can increase [^{11}C]ABP688 binding by up to 30%. Therefore PET image, rather than simply indicating tissue concentrations of neuroreceptors, can capture functional aspects of neuroreceptors in their native environment (Zimmer et al. 2015).

Moderate-strong mGluR5 immunoreactivity in balloon cells from FCD type IIb has been previously described (Aronica et al. 2003). In contrast, most balloon cells and dysmorphic neurons in the tissue obtained in our series had negative or weak mGluR5 immunoreactivity (Fig. 4), with a moderate-strongly stained neuropil and strong immunoreactivity in neurons that had a normal morphology within the periphery of resected tissue. Although the small number of patients in both series (11 in Aronica et al. (2003) and 4 in our study) does not allow for clear conclusions concerning these findings, it is interesting to note some differences between FCD IIb patients in these series. Mean age at surgery being much earlier (18 vs. 37) and proportion of seizure-free patients being much lower (50% vs. 100%) in the previously reported series might suggest a more severe form of epilepsy requiring earlier intervention as compared to our adult series (all our operated patients with FCD IIb had surgery after age 25, compared to only 3/11 of theirs).

Keeping in mind that our cohort is very small and considering the clinical-pathological findings in both series, we could speculate that our patients fall into a subcategory of FCD IIb in which epilepsy is less severe. Tissue differences described here (such as predominantly negative or weak mGluR5 positive balloon cells) could potentially correlate with a better prognosis, and the same could be potentially true for the [^{11}C]ABP688 BP_{ND} abnormalities described here.

Because many of our patients in the present series will not have a surgical resection due to location within eloquent cortex, we unfortunately cannot expand the imaging-pathological contributions at this point. Furthermore, the regulation on the administration of radioligands in research by Health Canada does not allow us to prospectively recruit patients younger than 18 y/o, making it unfeasible to design a prospective comparison to clarify these differences.

Indeed, an important limitation of our study is the small number of patients evaluated. While we attempted to control for potential confounds of particular relevance for mGluR5 imaging (from cigarette smoking to depression), a larger sample size may allow more robust comparisons and more specific characterization of lesional and extralesional abnormalities.

In conclusion, we have shown for the first time in vivo imaging of mGluR5 availability in patients with epilepsy and an underlying FCD. Using [^{11}C]ABP688 PET, we have demonstrated that binding is reduced in these lesions as compared to homotopic areas in healthy controls. Our findings, albeit derived from a small number of patients, support future studies on the evaluation of [^{11}C]ABP688 PET for diagnosis of occult malformations in patients with a negative MRI. Additional analysis comparing in vivo [^{11}C]ABP688 BPND to ex vivo analyses of protein quantification and function in different types of lesions resected from epilepsy patients may further elucidate the role of mGluR5 in epileptogenicity and epileptogenesis, particularly in malformations of cortical development. [^{11}C]ABP688 PET could shed light on more complex phenotypes related to mGluR5 dysfunction, including acquired forms of epilepsy, as well as neurodegenerative diseases, psychiatric conditions, and Fragile X chromosome syndrome, which can also be associated with seizures. Finally, mGluR5 imaging could potentially be used as an imaging biomarker for epileptogenesis in other forms of acquired epilepsies that can be targeted with disease modifying therapies.

Supplementary Material

Supplementary material can be found at: http://www.cercor.oxfordjournals.org/

Funding

The Savoy Foundation for Epilepsy (www.savoy-foundation.ca) (pilot project grant to E.K. and P.R.N. and PhD studentship to J.M.D.), and partially by the American Epilepsy Society (www.aesnet.org) (Early Career Physician Scientist Award to E.K.), Canadian Institutes of Health Research (CIHR) (www.cihr-irsc.gc.ca) (MOP-115131 to P.R.N. and MOP-93614 to E.K.), and the Fonds de la recherche en santé du Québec (www.frqs.gouv.qc.ca) (P.R.N., chercheur boursier).

Notes

Conflict of Interest: The authors declare that they have no conflict of interest.

References

Akbar MT, Rattray M, Powell JF, Meldrum BS. 1996. Altered expression of group I metabotropic glutamate receptors in the hippocampus of amygdala-kindled rats. Mol Brain Res. 43:105–116.

Ametamey SM, Treyer V, Streffer J, Wyss MT, Schmidt M, Blagoev M, Hintermann S, Auberson Y, Gasparini F, Fischer UC, et al. 2007. Human PET studies of metabotropic glutamate receptor subtype 5 with ^{11}C-ABP688. J Nucl Med. 48: 247–252.

Anwyl R. 1999. Metabotropic glutamate receptors: electrophysiological properties and role in plasticity. Brain Res Rev. 29:83–120.

Aronica E, Gorter JA, Jansen GH, van Veelen CW, van Rijen PC, Ramkema M, Troost D. 2003. Expression and cell distribution of group I and group II metabotropic glutamate receptor subtypes in taylor-type focal cortical dysplasia. Epilepsia. 44: 785–795.

Benjamini Y, Krieger AM, Yekutieli D. 2006. Adaptive linear step-up procedures that control the false discovery rate. Biometrika. 93:491–507.

Bianchi MT, Alexander BM, Cash SS. 2009. Incorporating uncertainty into medical decision making: an approach to unexpected test results. Med Decis Making. 29:116–124.

Blumcke I, Thom M, Aronica E, Armstrong DD, Vinters HV, Palmini A, Jacques TS, Avanzini G, Barkovich AJ, Battaglia G, et al. 2011. The clinicopathologic spectrum of focal cortical dysplasias: a consensus classification proposed by an ad hoc Task Force of the ILAE Diagnostic Methods Commission. Epilepsia. 52:158–174.

Catania MV, D'Antoni S, Bonaccorso CM, Aronica E, Bear MF, Nicoletti F. 2007. Group I metabotropic glutamate receptors: a role in neurodevelopmental disorders? Mol Neurobiol. 35: 298–307.

Chassoux F, Devaux B, Landré E, Turak B, Nataf F, Varlet P, Chodkiewicz J-P, Daumas-Duport C. 2000. Stereoelectroencephalography in focal cortical dysplasia A 3D approach to delineating the dysplastic cortex. Brain. 123:1733–1751.

Choi H, Kim YK, Oh SW, Im HJ, Hwang do W, Kang H, Lee B, Lee YS, Jeong JM, Kim EE, et al. 2014. In vivo imaging of mGluR5 changes during epileptogenesis using [^{11}C]ABP688 PET in pilocarpine-induced epilepsy rat model. PLoS One. 9:e92765.

Chugani DC, Ackermann RF, Phelps ME. 1988. In vivo [3H] spiperone binding: evidence for accumulation in corpus striatum by agonist-mediated receptor internalization. J Cereb Blood Flow Metab. 8:291–303.

Conn PJ, Pin JP. 1997. Pharmacology and functions of metabotropic glutamate receptors. Annu Rev Pharmacol Toxicol. 37: 205–237.

Daggett L, Sacaan A, Akong M, Rao S, Hess S, Liaw C, Urrutia A, Jachec C, Ellis S, Dreessen J. 1995. Molecular and functional characterization of recombinant human metabotropic glutamate receptor subtype 5. Neuropharmacology. 34:871–886.

Dale AM, Fischl B, Sereno MI. 1999. Cortical surface-based analysis. I. Segmentation and surface reconstruction. NeuroImage. 9:179–194.

DeLorenzo C, DellaGioia N, Bloch M, Sanacora G, Nabulsi N, Abdallah C, Yang J, Wen R, John Mann J, Krystal JH, et al. 2014. In vivo ketamine-induced changes in [^{11}C]ABP688 binding to metabotropic glutamate receptors subtype 5. Biol Psychiatry. 77:266–275.

Deschwanden A, Karolewicz B, Feyissa AM, Treyer V, Ametamey SM, Johayem A, Burger C, Auberson YP, Sovago J, Stockmeier CA, et al. 2011. Reduced metabotropic glutamate receptor 5 density in major depression determined by [(11)C]ABP688 PET and postmortem study. Am J Psychiatry. 168:727–734.

Desikan RS, Segonne F, Fischl B, Quinn BT, Dickerson BC, Blacker D, Buckner RL, Dale AM, Maguire RP, Hyman BT, et al. 2006. An automated labeling system for subdividing the human cerebral cortex on MRI scans into gyral based regions of interest. NeuroImage. 31:968–980.

DuBois JM, Rousset OG, Rowley J, Porras-Betancourt M, Reader AJ, Labbe A, Massarweh G, Soucy JP, Rosa-Neto P, Kobayashi E. 2016. Characterization of age/sex and the regional distribution of mGluR5 availability in the healthy human brain measured by high-resolution [(11)C]ABP688 PET. Eur J Nucl Med Mol Imaging. 43:152–162.

During MJ, Spencer DD. 1993. Extracellular hippocampal glutamate and spontaneous seizure in the conscious human brain. Lancet. 341:1607–1610.

Elmenhorst D, Minuzzi L, Aliaga A, Rowley J, Massarweh G, Diksic M, Bauer A, Rosa-Neto P. 2010. In vivo and in vitro validation of reference tissue models for the mGluR(5) ligand [(11)C]ABP688. J Cereb Blood Flow Metab. 30:1538–1549.

Fischl B, Dale AM. 2000. Measuring the thickness of the human cerebral cortex from magnetic resonance images. Proc Natl Acad Sci USA. 97:11050–11055.

Fischl B, Salat DH, Busa E, Albert M, Dieterich M, Haselgrove C, van der Kouwe A, Killiany R, Kennedy D, Klaveness S, et al. 2002. Whole brain segmentation: automated labeling of neuroanatomical structures in the human brain. Neuron. 33: 341–355.

Fischl B, Sereno MI, Dale AM. 1999a. Cortical surface-based analysis. II: Inflation, flattening, and a surface-based coordinate system. NeuroImage. 9:195–207.

Fischl B, Sereno MI, Tootell RBH, Dale AM. 1999b. High-resolution intersubject averaging and a coordinate system for the cortical surface. Hum Brain Mapp. 8:272–284.

Greve DN, Fischl B. 2009. Accurate and robust brain image alignment using boundary-based registration. NeuroImage. 48:63–72.

Greve DN, Svarer C, Fisher PM, Feng L, Hansen AE, Baare W, Rosen B, Fischl B, Knudsen GM. 2014. Cortical surface-based analysis reduces bias and variance in kinetic modeling of brain PET data. NeuroImage. 92:225–236.

Greve DN, Van der Haegen L, Cai Q, Stufflebeam S, Sabuncu MR, Fischl B, Brysbaert M. 2013. A surface-based analysis of language lateralization and cortical asymmetry. J Cogn Neurosci. 25:1477–1492.

Gunn RN, Lammertsma AA, Hume SP, Cunningham VJ. 1997. Parametric imaging of ligand-receptor binding in PET using a simplified reference region model. NeuroImage. 6:279–287.

Hagler DJ Jr, Saygin AP, Sereno MI. 2006. Smoothing and cluster thresholding for cortical surface-based group analysis of fMRI data. NeuroImage. 33:1093–1103.

Hefti K, Holst SC, Sovago J, Bachmann V, Buck A, Ametamey SM, Scheidegger M, Berthold T, Gomez-Mancilla B, Seifritz E, et al. 2013. Increased metabotropic glutamate receptor subtype 5 availability in human brain after one night without sleep. Biol Psychiatry. 73:161–168.

Hubbard JA, Szu JI, Yonan JM, Binder DK. 2016. Regulation of astrocyte glutamate transporter-1 (GLT1) and aquaporin-4 (AQP4) expression in a model of epilepsy. Exp Neurol. 283A: 85–96.

Innis RB, Cunningham VJ, Delforge J, Fujita M, Gjedde A, Gunn RN, Holden J, Houle S, Huang SC, Ichise M, et al. 2007. Consensus nomenclature for in vivo imaging of reversibly binding radioligands. J Cereb Blood Flow Metab. 27: 1533–1539.

Kirschstein T, Bauer M, Müller L, Rüschenschmidt C, Reitze M, Becker AJ, Schoch S, Beck H. 2007. Loss of metabotropic glutamate receptor-dependent long-term depression via down-regulation of mGluR5 after status epilepticus. J Neurosci. 27: 7696–7704.

Lammertsma AA, Bench CJ, Hume SP, Osman S, Gunn K, Brooks DJ, Frackowiak RS. 1996. Comparison of methods for analysis of clinical [^{11}C]raclopride studies. J Cereb Blood Flow Metab. 16:42–52.

Lamparello P, Baybis M, Pollard J, Hol EM, Eisenstat DD, Aronica E, Crino PB. 2007. Developmental lineage of cell types in cortical dysplasia with balloon cells. Brain. 130: 2267–2276.

Merlin LR. 2002. Differential roles for mGluR1 and mGluR5 in the persistent prolongation of epileptiform bursts. J Neurophysiol. 87:621–625.

Meurs A, Clinckers R, Ebinger G, Michotte Y, Smolders I. 2008. Seizure activity and changes in hippocampal extracellular glutamate, GABA, dopamine and serotonin. Epilepsy Res. 78: 50–59.

Milella M, Reader A, Albrechtsons D, Minuzi L, Soucy J, Benkelfat C. 2011. Human PET validation study of reference tissue models for the mGluR5 ligand [11 C] ABP688, Society for Neuroscience Annual Meeting. Washington, DC.

Morey RA, Petty CM, Xu Y, Hayes JP, Wagner HRII, Lewis DV, LaBar KS, Styner M, McCarthy G. 2009. A comparison of automated segmentation and manual tracing for quantifying hippocampal and amygdala volumes. NeuroImage. 45:855–866.

Palmini A, Gambardella A, Andermann F, Dubeau F, da Costa JC, Olivier A, Tampieri D, Gloor P, Quesney F, Andermann E. 1995. Intrinsic epileptogenicity of human dysplastic cortex as suggested by corticography and surgical results. Ann Neurol. 37:476–487.

R Core Team. 2013.R: a language and environment for statistical computing. Vienna: R Foundation for Statistical Computing.

Rousset OG, Ma Y, Evans AC. 1998. Correction for partial volume effects in PET: principle and validation. J Nucl Med. 39: 904–911.

Rowley HL, Marsden CA, Martin KF. 1997. Generalised seizure-induced changes in rat hippocampal glutamate but not GABA release are potentiated by repeated seizures. Neurosci Lett. 234:143–146.

Taylor DC, Falconer MA, Bruton CJ, Corsellis JA. 1971. Focal dysplasia of the cerebral cortex in epilepsy. J Neurol Neurosurg Psychiatry. 34:369–387.

Thomas BA, Erlandsson K, Modat M, Thurfjell L, Vandenberghe R, Ourselin S, Hutton BF. 2011. The importance of appropriate partial volume correction for PET quantification in Alzheimer's disease. Eur J Nucl Med Mol Imaging. 38:1104–1119.

Treyer V, Streffer J, Wyss MT, Bettio A, Ametamey SM, Fischer U, Schmidt M, Gasparini F, Hock C, Buck A. 2007. Evaluation of the metabotropic glutamate receptor subtype 5 using PET and ^{11}C-ABP688: assessment of methods. J Nucl Med. 48: 1207–1215.

van Velden FH, Kloet RW, van Berckel BN, Buijs FL, Luurtsema G, Lammertsma AA, Boellaard R. 2009. HRRT versus HR+ human brain PET studies: an interscanner test-retest study. J Nucl Med. 50:693–702.

van Wieringen J-P, Booij J, Shalgunov V, Elsinga P, Michel MC. 2013. Agonist high-and low-affinity states of dopamine D2 receptors: methods of detection and clinical implications. Naunyn-Schmiedeberg's Arch Pharmacol. 386:135–154.

Vidal B, Sebti J, Verdurand M, Fieux S, Billard T, Streichenberger N, Troakes C, Newman-Tancredi A, Zimmer L. 2016. Agonist and antagonist bind differently to 5-HT 1A receptors during Alzheimer's disease: a post-mortem study with PET radiopharmaceuticals. Neuropharmacology. 109:88–95.

Zimmer ER, Parent MJ, Cuello AC, Gauthier S, Rosa-Neto P. 2014. MicroPET imaging and transgenic models: a blueprint for Alzheimer's disease clinical research. Trends Neurosci. 37: 629–641.

Zimmer ER, Parent MJ, Leuzy A, Aliaga A, Aliaga A, Moquin L, Schirrmacher ES, Soucy J-P, Skelin I, Gratton A. 2015. Imaging in vivo glutamate fluctuations with [^{11}C] ABP688: a GLT-1 challenge with ceftriaxone. J Cereb Blood Flow Metab. 35:1169–1174.